Ab initio modeling of spin and charge ordering and lattice dynamics in $CaFeO_3$ crystals

V. E. Alexandrov,[1,a)] E. A. Kotomin,[1,2] J. Maier,[1] and R. A. Evarestov[3]
[1]*Max-Planck-Institut für Festkörperforschung, Heisenbergstrasse 1, D-70569 Stuttgart, Germany*
[2]*Institute for Solid State Physics, University of Latvia, Riga LV-1063, Latvia*
[3]*Department of Quantum Chemistry, St. Petersburg State University, 26 Universitetskiy Prospekt, Stary Peterhof 198504, Russia*

(Received 27 August 2008; accepted 28 October 2008; published online 3 December 2008)

Results of first-principles simulations on both orthorhombic and monoclinic phases of $CaFeO_3$ crystal are presented. The obtained atomic structures are consistent with x-ray diffraction data. The transition from a metallic orthorhombic to a narrow-gap semiconducting monoclinic phase is ascribed to the larger distortion of the Fe–O–Fe bond angle in the latter case. Calculations of Raman and optic active phonon modes at the Γ point of the Brillouin zone are performed and discussed. The isotopic substitution technique is applied to analyze the vibration modes obtained. The found charge/spin disproportionation is analyzed and compared with available experimental estimates.
 [DOI: 10.1063/1.3030976]

Diverse properties of transition-metal oxides have initiated a long-standing scientific interest and promoted a great deal of intensive studies. In recent years, many of these oxides, in particular, iron- and manganese-based ABO_3-type perovskites, have attracted a lot of attention in connection with ordering of charge, spin, or orbital degrees of freedom.[1,2] In this respect, $CaFeO_3$ is a fascinating solid in which the change from metallic to semiconducting behavior takes place because of the phase transition from the room-temperature orthorhombic (space group *Pbnm*) to a monoclinic (space group $P2_1/n$) modification that is stable below 290 K.[3] Such a metal-insulator transition is accompanied by a charge disproportionation between two inequivalent iron ions, as revealed by Mössbauer spectroscopy.[4] However, the degree of this disproportionation is rather unclear. In order to probe the magnetic structure, neutron-power diffraction has recently been applied.[3] Despite the fact that absolute values of the magnetic moments on the two iron sites in the monoclinic phase vary largely with the model of magnetic arrangement (spiral or sinusoidal), a considerable spin difference between two Fe ions is reproduced in both models.

There were only a few theoretical attempts to examine properties of both $CaFeO_3$ phases. For instance, calculation of the electronic structure and magnetic properties has been performed by using the LSDA+U approach[5] containing two adjustable parameters. However, the arbitrariness in choosing these parameters is a crucial shortcoming of the method. Thus, the authors obtained rather large variations in the magnetic moments on the iron atoms depending on the parameter values.

Recently, the role of lattice dynamics in the formation of a charge-disproportioned state in $CaFeO_3$ has been addressed by means of temperature-dependent Raman spectroscopy.[6] The phonon modes have been analyzed as a function of temperature, and shell-model lattice-dynamical calculations have been performed in order to assign the obtained Raman modes along with the determination of their vibrational pattern.

In this article, we aim to provide the results of first-principles calculations of atomic structure and electronic and magnetic properties of $CaFeO_3$ as well as Γ-point vibrational frequencies. For this purpose, we have chosen the so-called hybrid B3PW exchange-correlation functional[7] which combines the nonlocal exact Fock exchange used in Hartree–Fock (HF) method and density functional theory (DFT) generalized gradient approximation exchange functionals using Becke's three parameter method as implemented in the linear combination of atomic orbitals (LCAO)-based CRYSTAL06 computer package.[8] Note that the application of a hybrid functional in the calculations of $CaFeO_3$ is necessary for reliable discrimination of small changes in the band gap and electronic properties[9] related to the $CaFeO_3$ phase transition as well as for analysis of the phonon modes.[10] We employed the Monkhorst–Pack[11] $8\times8\times6$ set of $\mathbf{k}$ points for the summation in the Brillouin zone as sufficiently large to obtain good agreement with experimental data on atomic structure and Raman frequencies. All atoms were treated on the all-electron level with the use of optimized basis sets [Ca,[12] Fe,[13] O[9]]. For a full optimization of the $CaFeO_3$ atomic

TABLE I. Optimized and experimental (Ref. 3) unit cell parameters a, b, and c (Å) and angle β (deg) for orthorhombic *Pbnm* and monoclinic $P2_1/n$ phases.

	Orthorhombic			Monoclinic			
Parameter	a	b	c	a	b	c	β
Calculation	5.330	5.346	7.565	5.317	5.349	7.562	90.001
Experiment	5.326	5.353	7.540	5.312	5.348	7.521	90.065

a)Electronic mail: v.alexandrov@fkf.mpg.de.

TABLE II. Optimized and experimental (Ref. 3) fractional atomic coordinates for orthorhombic *Pbnm* and monoclinic $P2_1/n$ phases.

		Calculation			Experiment		
Atom	Site	*x*	*y*	*z*	*x*	*y*	*z*
			Orthorhombic				
Ca	4*c*	0.995	0.033	0.250	0.995	0.033	0.250
Fe	4*b*	0.0	0.5	0.0	0.0	0.5	0.0
O(1)	8*d*	0.710	0.285	0.032	0.713	0.286	0.033
O(2)	4*c*	0.062	0.485	0.25	0.066	0.491	0.25
			Monoclinic				
Ca	4*e*	0.995	0.035	0.250	0.994	0.037	0.251
Fe(1)	2*d*	0.5	0.0	0.0	0.5	0.0	0.0
Fe(2)	2*c*	0.0	0.5	0.0	0.0	0.5	0.0
O(1)	4*e*	0.296	0.717	−0.032	0.300	0.720	−0.033
O(2)	4*e*	0.218	0.205	−0.032	0.219	0.206	−0.032
O(3)	4*e*	0.063	0.486	0.257	0.076	0.493	0.254

structures, we used the two-step iterative procedure in which the lattice parameters are optimized at fixed atomic positions, then atomic coordinates are optimized at fixed cell parameters, and this repeats until convergence criteria for both steps are fulfilled.

In Tables I and II the calculated and experimental lattice parameters and atomic coordinates are presented. Calculations were carried out for the ferromagnetic spin configuration with four unpaired electrons on each iron site which has been found to be the most favorable magnetic ordering. We found the monoclinic phase to be energetically more favorable (by ~0.25 eV) than the orthorhombic one, in agreement with the experimental observation that the monoclinic phase is a low-temperature phase. Importantly, the optimization of the hypothetical cubic phase in $Pm\bar{3}m$ space group symmetry yields an energy which is the highest among all modifications considered.

TABLE III. Mulliken population analysis of atomic net charge $(\alpha+\beta)$ and net spin $(\alpha-\beta)$.

			Orthorhombic		
Density	Ca	Fe		O(1)	O(2)
$\alpha+\beta$	1.75	2.25		−1.33	−1.34
$\alpha-\beta$	0.01	3.71		0.10	0.09
			Monoclinic			
Density	Ca	Fe(1)	Fe(2)	O(1)	O(2)	O(3)
$\alpha+\beta$	1.75	2.26	2.24	−1.33	−1.33	−1.34
$\alpha-\beta$	0.01	3.13	4.10	0.13	0.13	0.13
$\alpha-\beta$ [a]		2.40	3.90			
$\alpha-\beta$ (expt.[b])		2.48[c]/3.40[d]	3.47/5.02			

[a]LSDA+*U* calculation (Ref. 5) performed with the onsite Coulomb parameter U=0.4 Ry and the intra-atomic exchange parameter J=0.07 Ry.
[b]Reference 3.
[c]Spiral model for the interpretation of the neutron diffraction experiment (Ref. 3).
[d]Sinusoidal model.

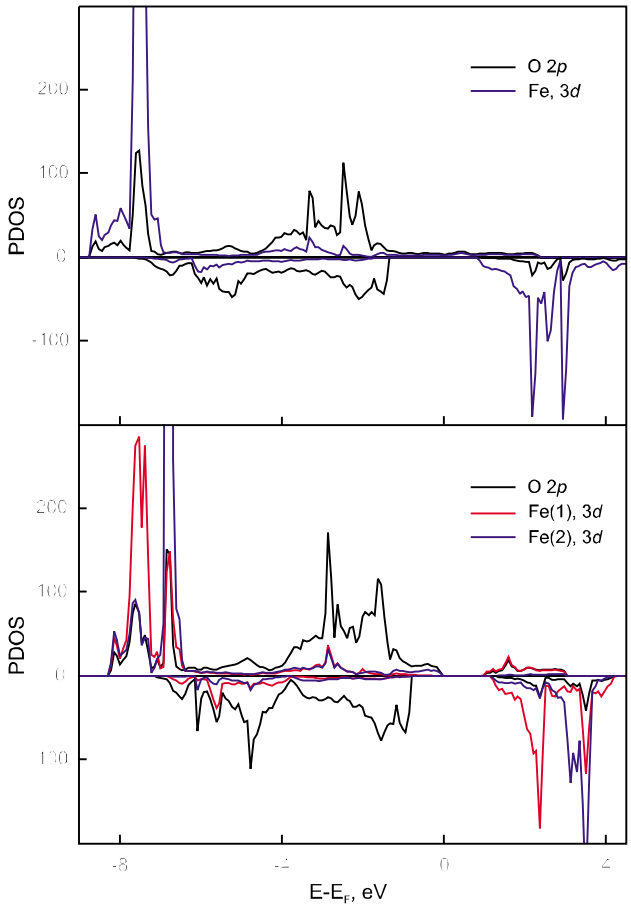

FIG. 1. (Color online) The density of electronic states projected onto Fe 3*d* and O 2*p* orbitals for orthorhombic (upper panel) and monoclinic (lower panel) phases of $CaFeO_3$ (projections are made onto only symmetrically inequivalent atoms).

As seen from Tables I and II, the orthorhombic modification is very slightly distorted from a cubic symmetry while the monoclinic one presents a slightly distorted orthorhombic phase. It should be mentioned that the Fe–O bond lengths in the monoclinic phase fall into two groups corresponding to two inequivalent Fe ions with the averaged Fe–O distances of 1.87 and 1.97 Å. This indicates two types of chemically different iron sites, although in the orthorhombic phase with all equivalent iron atoms the averaged Fe–O bond lengths group around 1.92 Å.

The results of Mulliken population analysis are given in Table III. It is seen that the atomic charges support the general idea of charge ordering in the monoclinic phase. However, the difference between Fe(1) and Fe(2) charges is very small. It should be noted that the degree of this charge disproportionation varies with the temperature[14] and our results, obtained formally at 0 K, are in line with those of the LSDA+*U* calculations.[5]

In contrast to small differences in charges, we observe a considerable splitting between spin densities on the two iron sites, corroborating the existence of spin ordering in the monoclinic phase. Such a significant difference in magnetic moments qualitatively agrees with Ref. 5 and the experimen-

TABLE IV. Calculated and experimentally observed Raman active modes (cm^{-1}) at 15 K (given in the footnote, Ref. 6).

A_g	146.0[a]	157.8	214.8[b]	244.5	266.5	298.1	352.1	374.1	402.0	456.8	464.4	624.5
B_g	155.6	176.6	185.0[c]	231.1	247.2	317.6[d]	370.1	381.5	445.9	487.0	583.7	615.4

[a]154.
[b]219.
[c]199.
[d]306.

tal estimates from neutron diffraction data[3] as seen from Table III. It is worth anticipating that the precise determination of absolute values of magnetic moments on Fe atoms from the neutron diffraction experiments[3] is difficult because, first, various experimental models (spiral or sinusoidal) lead to different results and, second, the obtained experimental spectra exhibit rather broadened magnetic peaks. Nevertheless, both experiment and our calculations reveal very distinct magnetic moments on the two iron sites in the monoclinic phase.

For the analysis of $CaFeO_3$ electronic properties, we calculated the band structure and projected density of electronic states for both structural modifications. The densities of states projected onto Fe $3d$ and O $2p$ states demonstrate a strong mixing of these states in the orthorhombic phase, being responsible for the metallic behavior, while this mixing decreases in the monoclinic phase due to the larger lattice distortion and change in the Fe–O–Fe angles, thus opening a small band gap ($\sim$0.9 eV). The projected densities of states (PDOSs) for spin up and spin down electrons for both $CaFeO_3$ phases are shown in Fig. 1. Note that there are obvious similarities between orthorhombic $CaFeO_3$ and cubic $SrFeO_3$ (Ref. 15) pertaining to the magnetic structures and electronic properties. Thus, both crystals have ferromagnetic spin arrangement with close magnetic moments on Fe atoms ($3.71\mu_B$ versus $3.79\mu_B$, respectively) and their electronic conductivity is caused by an effective mixing of Fe $3d$ and O $2p$ orbitals in the vicinity of the Fermi level.

The results of lattice-dynamics simulations were obtained within the harmonic approximation as implemented in the CRYSTAL06 code (for more details see Refs. 10 and 16). Here, the reader should just bear in mind that the vibrational frequencies at the Γ point of the Brillouin zone are obtained by diagonalizing the mass-weighted Hessian matrix with elements $W_{ij}=H_{ij}/\sqrt{M_iM_j}$, where M_i and M_j are the masses of the atoms with i and j coordinates, respectively. For the analysis of atomic contributions to the phonon modes in a given frequency range, the isotopic substitution technique was applied by changing the atomic masses in the mass-weighted Hessian when the latter is obtained.

As mentioned above, the $CaFeO_3$ monoclinic phase belongs to the $P2_1/n$ space group whose reducible representations at the Γ point in the basis of the Cartesian atomic coordinates in the unit cell can, according to the C_{2h} point group symmetry, be decomposed as

$$\Gamma_{\text{total}} = 12A_g + 18A_u + 12B_g + 18B_u,$$

where A_g and B_g are Raman active and A_u and B_u are infrared active modes. Three modes are acoustic (pure translations) whose calculated frequencies deviate from zero by only 1–2 cm^{-1}, reflecting the reasonable accuracy in the phonon calculations.

Tables IV and V compile the Raman and optical vibration frequencies, respectively, of monoclinic $CaFeO_3$ labeled by symmetry of each mode. Raman active modes are compared with those experimentally observed in Ref. 6 at 15 K. Our analysis of the Raman normal modes has led to the same vibrational patterns as revealed by using the lattice-dynamical calculations based on a semiempirical approach.[6]

As anticipated earlier, the isotopic substitution is a helpful tool for the identification of the vibrational pattern of the modes. Figure 2 illustrates isotopic effects related to the substitution of ^{40}Ca by ^{42}Ca (a), ^{56}Fe by ^{58}Fe (b), and ^{16}O by ^{18}O (c). It is clearly seen that for the atoms of each element there is a region where these atoms give a predominant contribution. Thus, one recognizes that Ca participates mainly in low-frequency modes (around 220 cm^{-1}) while Fe participates particularly in the modes with frequencies of 453 and 458 cm^{-1}. It is also observed that isotopic shifts are generally the largest for O atoms, their involvement into the vibrations steadily increasing when going to higher frequencies.

To summarize, we performed the first-principles simulations of orthorhombic and monoclinic $CaFeO_3$ phases in the framework of the hybrid HF-DFT LCAO approach. The calculated atomic structures are in very good agreement with the neutron-powder diffraction data. Calculations of PDOS revealed the transition from the metallic orthorhombic phase to the semiconducting monoclinic one due to the larger lattice distortion in the latter case, giving rise to reduced overlap between Fe $3d$ and O $2p$ states near the Fermi level. The disproportionation between two nonequivalent Fe atoms in the unit cell in the monoclinic phase was found both for charges and spin densities to be much more pronounced for the latter quantity. In addition, we calculated Brillouin zone-center phonon modes (Raman and optical) and analyzed the vibrational pattern.

TABLE V. Calculated optical active modes (cm^{-1}).

A_u	139.7	167.1	173.0	176.2	219.4	227.2	244.1	273.3	307.3	322.1	351.7	409.1	458.3	476.4	535.7	544.7	549.1
B_u	151.8	167.6	199.8	214.1	229.1	232.3	274.2	300.6	325.6	381.2	411.2	411.2	452.6	524.2	557.7	565.5	

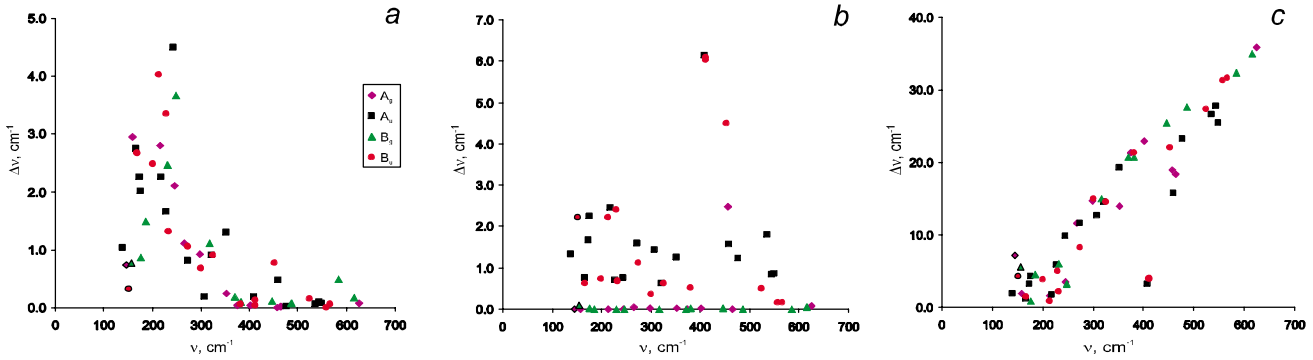

FIG. 2. (Color online) The isotopic effects for three types of isotopic substitutions: (a) ^{42}Ca replacing ^{40}Ca; (b) ^{58}Fe replacing ^{56}Fe; (c) ^{18}O replacing ^{16}O.

The authors are thankful to A. Fujimori and S. Ghosh for providing information on the Raman experiments. A. Kuzmin, J. Purans, and R. Merkle are acknowledged for valuable discussions.

[1] C. Israel, M. J. Calderon, and N. D. Mathur, Mater. Today **10**, 24 (2007).
[2] J. B. Goodenough and J.-S. Zhou, J. Mater. Chem. **17**, 2394 (2007).
[3] P. M. Woodward, D. E. Cox, E. Moshopoulou, A. W. Sleight, and S. Morimoto, Phys. Rev. B **62**, 844 (2000).
[4] M. Takano, N. Nakanishi, Y. Takeda, S. Naka, and T. Takada, Mater. Res. Bull. **12**, 923 (1977).
[5] J. B. Yang, M. S. Kim, Q. Cai, X. D. Zhou, H. U. Anderson, W. J. James, and W. B. Yelon, J. Appl. Phys. **97**, 10A312 (2005).
[6] S. Ghosh, N. Kamaraju, M. Seto, A. Fujimori, Y. Takeda, S. Ishiwata, S. Kawasaki, M. Azuma, M. Takano, and A. K. Sood, Phys. Rev. B **71**, 245110 (2005).
[7] A. D. Becke, J. Chem. Phys. **98**, 5648 (1993).
[8] R. Dovesi, V. R. Saunders, C. Roetti, R. Orlando, C. M. Zicovich-Wilson, F. Pascale, B. Civalerri, K. Doll, N. M. Harrison, I. J. Bush, Ph. D'Arco, and M. Llunell, CRYSTAL06 User's Manual, University of Torino, Torino, 2006.
[9] S. Piskunov, E. Heifets, R. I. Eglitis, and G. Borstel, Comput. Mater. Sci. **29**, 165 (2004).
[10] C. M. Zicovich-Wilson, F. Pascale, C. Roetti, V. R. Saunders, R. Orlando, and R. Dovesi, J. Comput. Chem. **25**, 1873 (2004).
[11] H. J. Monkhorst and J. D. Pack, Phys. Rev. B **13**, 5188 (1976).
[12] M. Catti, R. Dovesi, A. Pavese, and V. R. Saunders, J. Phys.: Condens. Matter **3**, 4151 (1991).
[13] M. Catti, G. Valerio, and R. Dovesi, Phys. Rev. B **51**, 7441 (1995).
[14] M. Takano, N. Nakanishi, Y. Takeda, and S. Naka, J. Phys. (Paris), Colloq. **40**, C2–313 (1979).
[15] V. E. Alexandrov, J. Maier, and R. A. Evarestov, Phys. Rev. B **77**, 075111 (2008).
[16] F. Pascale, C. M. Zicovich-Wilson, F. Lopez Gejo, B. Civalleri, R. Orlando, and R. Dovesi, J. Comput. Chem. **25**, 888 (2004).